© 2019. Published by The Company of Biologists Ltd | Journal of Experimental Biology (2019) 222, jeb187484. doi:10.1242/jeb.187484

RESEARCH ARTICLE

Zonation of Ca^{2+} transport and enzyme activity in the caeca of rainbow trout – a simple structure with complex functions

Melanie Williams, Domenico Barranca and Carol Bucking*

ABSTRACT

Trout caeca are vermiform structures projecting from the anterior intestine of the gastrointestinal tract. Despite their simple gross morphology, these appendages are physically distinct along the anterior–posterior axis, and ultrastructural evidence suggests zonation of function within the structures. Individual caeca from three sections (anterior, middle and posterior) were removed from the intestine of freshwater rainbow trout and investigated for ion transport and enzyme activity. Ca^{2+} absorption appeared as a combination of active and passive movement, with Michaelis–Menten kinetics observable under symmetrical conditions, and was inhibited by several pharmacological agents (ouabain, La^{3+} and a calmodulin antagonist). There was a decrease in ion transport function from adjacent to the intestine (proximal) to the distal tip of each caecum, along with decreasing transport from anterior to posterior for the proximal portion alone. Feeding increased the J_{Max} and K_M for Ca^{2+} absorption within all sections, whereas ion-poor water (IPW) exposure further increased the J_{Max} and K_M for Ca^{2+} transport in the anterior and middle sections. Increased Na^+/K^+-ATPase (NKA) and citrate synthase (CS) activity rates paralleled trends seen in Ca^{2+} transport. Feeding in freshwater and IPW exposure increased the glycolytic capacity of the caeca via increased pyruvate kinase (PK) and decreased lactate dehydrogenase (LDH) activity, while amino acid metabolism increased with IPW exposure through increased glutamate dehydrogenase (GDH) activity. Overall, feeding and IPW exposure each altered ionoregulation within the caeca of freshwater rainbow trout in a zone-specific pattern, with the anterior and proximal portions of the caeca being most affected. Increased carbohydrate and protein metabolism fueled the increased ATP demand of NKA through CS.

KEY WORDS: Digestion, Gastrointestinal tract, Ionoregulation, Ion-poor water, Metabolic enzymes

INTRODUCTION

Blind-ended digitations known as caeca are associated with the gastrointestinal tract of slightly more than half of known fish species (Hossain and Dutta, 1996). These projections are composed of four tissue layers: the predominant mucosa (the epithelia; Anderson, 1986), a reduced submucosa (the lamina propria and stratum compactum; Williams and Nickol, 1989), muscularis (the longitudinal and circular muscle) and serosa (the connective tissue). Moreover, the mucosa contains several cell types: goblet cells responsible for mucous secretion, absorptive columnar cells (Anderson, 1986; Williams and Nickol, 1989; Abaurrea-Equisoaín and Ostos-Garrido, 1996), secretory cells (Anderson, 1986; Williams and Nickol, 1989) and immune cells (leucocytes, macrophages; Williams and Nickol, 1989). The tissue of the caeca and the intestine (from where they originate) is generally similar (e.g. Burnstock, 1959; Kapoor et al., 1976; Buddington and Diamond, 1987; Chen et al., 2006; Faulk et al., 2007; Zizza and Desantis, 2011). However, the stratum compactum and muscularis are thinner (~30 µm) compared with the intestine proper (~45 µm; Anderson, 1986; Williams and Nickol, 1989). In addition, the number of goblet cells in the caeca can be dissimilar from the intestine proper (Williams and Nickol, 1989; Hossain and Dutta, 1996) depending on species. Heterogeneity of dispersion, from proximal base to distal tip, can also be present for both goblet cells (Jansson and Olsson, 1960) and absorptive cells (Anderson, 1986). However, when comparing anterior with posterior caeca, a single investigation failed to reveal structural zonation (Williams and Nickol, 1989).

Caeca structure has informed hypotheses about their function, which have included digestion and nutrient absorption (e.g. Jansson and Olsson, 1960; Bauermeister et al., 1979; Sire et al., 1981), as well as fermentation and storage (Buddington and Diamond, 1987). Other suggested roles include ion and water absorption (e.g. Bogé et al., 1988; Grosell et al., 2009). In fact, cells in the caeca of rainbow trout have lamellar structures, which appear to be in-foldings of the plasma membrane, associated with mitochondria as observed in other ion-transporting cells (Ezeasor and Stokoe, 1981; Giffard-Mena et al., 2006). As such, physiological and morphological studies have associated the caeca with ion and water transport, particularly during salinity acclimation [i.e. freshwater (FW) versus seawater (SW); e.g. Bogé et al., 1988; Abaurrea-Equisoaín and Ostos-Garrido, 1996; Veillette et al., 2005; Grosell et al., 2009]. Of particular interest to salt and water balance, Na^+/K^+-ATPase (NKA) uses ATP to generate electrochemical gradients, enabling ionic and osmotic regulation required to maintain homeostasis (Karnaky, 1986; McCormick, 1995; Brijs et al., 2015). In fact, enterocyte NKA activity is upregulated in SW compared with FW (Evans et al., 2005; Edwards and Marshall, 2012), directly fueling increased transport across the intestine; a phenomenon present in the caeca themselves (e.g. Veillette et al., 2005; Schwarz and Allen, 2014). In contrast, the impact of transitions to ion-poor water (IPW), which results in several osmoregulatory compensations, on the function of caeca is unknown. This is despite variations in FW ion levels (e.g. 4 mmol Ca^{2+} l^{-1} versus 10 µmol Ca^{2+} l^{-1}; Marier et al., 1979) based on numerous geological and environmental factors. In fact, depending on water body location, fish may encounter a range of water compositions from very hard to naturally soft throughout their life cycle.

Finally, the gut of fish has documented zonation in terms of salt and water balance (e.g. Bucking and Wood, 2006a; Whittamore, 2012), transporter expression (e.g. Grosell et al., 2007; Bucking and

Department of Biology, York University, Toronto, Ontario, Canada, M3J 1P3.

*Author for correspondence (cbucking@yorku.ca)

C.B., 0000-0003-3655-426X

Received 24 June 2018; Accepted 7 February 2019

Journal of Experimental Biology (2019) 222, jeb187484. doi:10.1242/jeb.187484

Wood, 2012; Li et al., 2014), and nutrient transport and enzyme activities (e.g. Collie, 1985; Mommsen et al., 2003; Bucking and Wood, 2012; Rubino et al., 2014; Turner and Bucking, 2017). Indeed, the caeca of rainbow trout display the highest activities of several metabolic enzymes, including glutamate dehydrogenase (GDH), lactate dehydrogenase (LDH) and citrate synthase (CS) (Mommsen et al., 2003). However, it is unclear whether there is zonation of enzyme activity or transport within caeca and what responses these appendages have to abiotic factors such as salinity. FW–SW transitions correlate with alterations in gut metabolic enzyme activities in teleost fish [e.g. GDH, Chew et al., 2010; LDH and pyruvate kinase (PK), Ransberry et al., 2015], suggesting an environmentally dependent role for caeca in ATP production. Whether these effects are correlated with ion transport and energy demand is also unclear.

Despite previous assertions that the caeca were mere extensions of the intestine proper, detailed histological investigations suggest a heterogeneity of cells along individual caeca from the proximal base to the distal tip. Hence, our study investigated Ca^{2+} transport zonation within and between individual caeca using the scanning ion electrode technique (SIET) as well as pharmacological interventions such as $LaCl_3$ or W7 [*N*-(6-aminohexyl)5-chloro-1-naphthalene sulfonamide (a calmodulin antagonist that inhibits Ca^{2+}-ATPase activity; Garrahan, 2018; Perry and Flik, 1988)]. Owing to their structure and function, we predicted region-specific ion transport along the individual caeca, mirroring epithelial cell distributions, but no zonation along the anterior–posterior axis. Furthermore, we predicted that zonation of enzyme activity (NKA and metabolic enzymes) would be present, correlating with ATP and transport demand within the organs. Finally, we tested the impact of environmental salinity to observe whether the function of caeca themselves was responsive. The effect of IPW on the caeca is unknown, but due to their role in salt and water balance in SW, they may be the source of needed salt absorption to compensate for lowered environmental concentrations. Hence, we predicted that IPW exposure would affect NKA and metabolic enzyme activity to support the increase in observed ion transport.

MATERIALS AND METHODS

Experiments were conducted under approved institutional animal care guidelines in accordance with federal mandates. All chemicals were purchased from Sigma-Aldrich unless otherwise noted.

Animals

Juvenile rainbow trout [*Oncorhynchus mykiss* (Walbaum 1792), ∼45 g] were obtained from Humber Springs Trout Hatchery (Orangeville, ON, Canada). Fish were transported to the laboratory and housed in 200 l opaque tanks supplied with flow-through, aerated, dechlorinated City of Toronto tap water ($[Na^+]$=590 µmol l^{-1}, $[Cl^-]$=920 µmol l^{-1}, $[Ca^{2+}]$=900 µmol l^{-1}, $[K^+]$=50 µmol l^{-1}, pH 7.4). Fish were fed daily with commercial trout pellets (∼3% body mass ration; Martin Mills Profishent, Elmira, ON, CA; ∼1.4 g per fish) and were held under a constant photoperiod (14 h:10 h light:dark). Following a period of laboratory acclimation, fish were fed daily at a set time and animals were randomly sampled from the tank 24 h following feeding (referred to as fed FW fish). Additionally, animals were also fasted in FW for 1 week and then sampled (referred to as unfed FW fish).

Ion-poor water exposure

For IPW exposures, animals were fed and the flow-through water supply to the tanks was abruptly changed to IPW ($[Na^+]$=20 µmol l^{-1}, $[Cl^-]$=40 µmol l^{-1}, $[Ca^{2+}]$=2 µmol l^{-1}, $[K^+]$=0.4 µmol l^{-1}, pH 7.4, temperature=13°C; measured at inflow). IPW water was generated through reverse osmosis of dechlorinated City of Toronto tap water. Removal of uneaten food (if any) 5 min following the designated feeding time eliminated any potential leaching of ions and subsequent alterations of IPW parameters. IPW-exposed animals were sampled following 24 h exposure (referred to as fed IPW fish).

An additional fed FW control group was used for comparison with the IPW animals. This was to determine whether the feeding results that we observed were repeatable. For this control group, the rainbow trout were held in FW, fed and then sampled 24 h following feeding as for the IPW fish.

Sampling

During sampling, all animals were terminally anesthetised with pH buffered tricaine methasulfonate [MS-222 (Sundel Laboratories Ltd, Canada); 0.5 g l^{-1}, buffered to pH 7.4 with NaOH prior to use]. Following this, the body wall was opened and the entire gut removed. The anterior intestine was identified based on the presence of ∼75 caecum structures and divided into three equal and proportional sections: the anterior, the middle and the posterior. Individual caeca were removed from the anterior, middle and posterior areas of the anterior intestine at the junction with the anterior intestine itself. These intact caeca from each section were then used for ion flux measurements, described below. The remaining caeca from each section were removed from the anterior intestine, visually divided in half and subsequently dissected into proximal (previous site of attachment to the anterior intestine) and distal (at the caeca tip) portions, which were each pooled within each section. These pooled tissue samples were immediately freeze-clamped in liquid nitrogen and placed in a −80°C freezer until enzyme analysis. The remaining anterior intestine was sampled with the absence of caeca (to obtain tissue from the intestine proper), as were gill filaments from the entire second and third gill arch and the whole kidney, freeze-clamped and stored at −80°C until analysis.

Ion transport

The scanning ion electrode technique (SIET) was used to measure ion flux across the mucosa as previously described (Rheault and O'Donnell, 2001; Nguyen and Donini, 2010). Each caecum was everted before measurement, filled with saline (described briefly in Table S1) delivered via PE-50 tubing attached to a 22-G needle and 1 ml syringe, and tied with thread, creating a taut, sealed caecum. The presence of leaks was excluded through visual inspection. During preparation, the tissues were incubated in ice-cold Cortland saline [123 mmol l^{-1} NaCl, 5 mmol l^{-1} KCl, 1.9 mmol l^{-1} $CaCl_2$, 1.0 mmol l^{-1} $MgSO_4$, 11.9 mmol l^{-1} $NaHCO_3$, 2.9 mmol l^{-1} NaH_2PO_4, 5.5 mmol l^{-1} glucose; pH 7.4 (adjusted to final pH with 1 mol l^{-1} NaOH)], but ion transport measurements were obtained at room temperature (22°C) and each individual caecum was filled and incubated in a series of solutions containing various concentrations of Ca^{2+} (Table S1). A schematic layout of Ca^{2+} measurements is found in Fig. S1.

For asymmetrical treatments, the internal serosal saline that filled the sac contained 0 µmol l^{-1} Ca^{2+}. The external bath $CaCl_2$ concentrations (0, 4, 8, 16, 32, 46, 68, 136, 275, 500 and 1000 µmol l^{-1}) were manipulated to determine transport kinetics (Table S1). The osmotic pressure between the mucosal and serosal baths was maintained through the addition of mannitol [3.2–1753 µmol l^{-1}; measured with an osmometer (Advanced Analytics, Fisher Scientific)]. Additionally, using unfed tissues, 200 µmol l^{-1}

$LaCl_3$ or 1 µmol l^{-1} W7 was added to the serosal and mucosal baths. W7 was dissolved in ethanol (100%; Fisher Scientific) and application of W7 never exceeded 0.1% vol/vol ethanol in the tissue bath. Ion transport measurements were made at the proximal portion of each caecum.

For symmetrical treatments, the mucosal and serosal bath Ca^{2+} concentrations were matched (0, 4, 8, 16, 32, 46, 68, 136, 275, 500 and 1000 µmol l^{-1}; Table S1). For this experiment, the PE-50 tubing was tied into the sac and heat-sealed between each measurement. The tubing was then re-opened, the sac drained and re-filled with a new Ca^{2+} concentration. This was repeated for each of the concentrations, which were applied in a random order. During the measurements of kinetic flux in unfed tissues, at 500 µmol l^{-1} mucosal and serosal Ca^{2+}, 200 µmol l^{-1} $LaCl_3$, 1 µmol l^{-1} W7 or 100 µmol l^{-1} ouabain was added in a random order and flux was measured following 10 min of incubation. Following each inhibitor, the tissues were bathed in inhibitor-free mucosal saline for 10 min and recovery of transport rates to pre-exposure values was verified. Interference from La^{3+}, W7 and ouabain on the ion-selective microelectrode (ISME) was not detected. Finally, ion transport measurements were made at the proximal and distal points of each caecum (along with a mid-point in the anterior caeca owing to their length) for tissues obtained from unfed FW animals only. For all other treatments, ion measurement were made at the proximal portion.

Measuring ion concentrations

To form ISMEs (tip diameter of 5–8 µm), glass capillaries (model TW150-4; WPI, Sarasota, FL, USA) were pulled on a P-97 Flaming-Brown horizontal micropipette puller (Sutter Instruments, Novato, CA, USA). The microelectrodes were then salinized [capillaries were heated to 350°C for 15 min and subsequently covered with a borosilicate dish containing *N*,*N*-dimethyltrimethylsilylamine (Fluka, Buchs, Switzerland; ∼1 µl per electrode) for 1 h at 350°C] before construction immediately before each use. The Ca^{2+}-selective microelectrodes were formed by front-filling with Calcium II ionophore cocktail (Fluka Chemical Co., Ronkonkoma, NY, USA) and backfilling with a 100 mmol l^{-1} $CaCl_2$ solution for a column length of 100–150 nm. The calibration solutions (100 and 1000 µmol l^{-1} $CaCl_2$) produced an average slope of 29±1.0 mV. Reference electrodes were constructed using a borosilicate glass microcapillary (model TW150-4; WPI) that was heated at one end to form a 45 deg bend and filled with 3 mol l^{-1} KCl solution containing 3% agar. The solution was allowed to harden, and the reference electrodes were stored in 3 mol l^{-1} KCl between uses. Both the ISME and a reference electrode were connected to a headstage (by an Ag/AgCl wire holder for the former and Ag/AgCl half-cell for the latter; WPI), which was in turn connected to an ion polarographic amplifier (IPA-2; Applicable Electronics, Forestdale, MA, USA). Automated scanning electrode technique software (ASET; Sciencewares, East Falmouth, MA, USA) was used to control an ISME mounted on a 3D micro-stepper motor manipulator (CMC-4; Applicable Electronics). Voltage gradients (ΔV in mV), measured between the intestinal mucosal surface and a set distance away from the tissue, were converted into ionic concentration gradients with the following formula:

$$\Delta C = C_B \times 10^{\left(\frac{\Delta V}{S}\right)} - C_B, \quad (1)$$

where ΔC is the concentration gradient between the tissue and the reference point (calculated in nmol l^{-1} cm^{-3}), C_B is the background ion concentration (recorded in nmol l^{-1}), ΔV is the voltage gradient (mV) and S is the slope of the electrode over a 10-fold difference in ion concentration (mV).

ΔC was then converted into flux using Fick's law of diffusion:

$$J_I = D_I(\Delta C)/\Delta X, \quad (2)$$

where J_I is the net flux (measured in nmol cm^{-2} min^{-1}), D_I is the diffusion coefficient of the measured ion (7.14×10^{-4} cm^2 min^{-1} for Ca^{2+}) and ΔX is the distance between the two points (cm).

Enzyme analysis

All intestinal enzymes were measured according to previously published methods. Before assays were run, pooled proximal and distal tissues from the anterior, middle and posterior caeca were individually ground into a fine powder with a mortar and pestle under liquid nitrogen and stored again at −80°C. Care was taken to ensure that the tissue did not thaw until placed in extraction buffer for enzyme analysis. Reactions were started by addition of tissue homogenization preparation and enzyme activity rates were determined as the maximal change in extinction at 340 nm owing to the oxidation or reduction of NADH or NAD using microplates read on a spectrophotometer (Biotek, Fisher Scientific) unless otherwise stated. Enzyme activity, defined as micromoles of substrate converted to product per minute (IU), at 25°C, was expressed per gram of intestinal tissue protein (determined by the Bradford method using a commercial kit; Bio-Rad) unless otherwise noted. Maximal activities were determined for each enzyme during optimization.

NKA (E.C. 3.6.3.9; e.g. Bucking et al., 2013; Turner and Bucking, 2017) activity was measured by placing an aliquot of ground tissue into homogenization buffer which was homogenized with a Wheaton overhead stirrer (with a modified pestle probe; Rochdale, UK) for 30 s. A supernatant was obtained following centrifugation (5000 ***g***) at 4°C for 30 s. The homogenization buffers [SEI buffer (150 mmol l^{-1} sucrose, 10 mmol l^{-1} EDTA, 50 mmol l^{-1} imidazole, pH 7.5); SEID buffer (0.5 g sodium deoxycholate in 100 ml SEI buffer)] and reaction buffers [salt solution (50 mmol l^{-1} NaCl, 10.5 mmol l^{-1} $MgCl_2$, 42 mmol l^{-1} KCl, 50 mmol l^{-1} imidazol), Solution A (50 mmol l^{-1} imidazole, 2.8 mmol l^{-1} PEP, 0.22 mmol l^{-1} NADH, 0.7 mmol l^{-1} ATP, 4 units ml^{-1} LDH, 5 units ml^{-1} PK), and Solution B (0.5 mmol l^{-1} ouabain in 10 ml Solution A)] were made fresh daily before use. Solutions and homogenized tissues were kept on ice until the assay was read. NKA activity was expressed in µmol ADP mg^{-1} protein h^{-1}.

An additional aliquot of the ground frozen tissue was added to four volumes of extract buffer [50 mmol l^{-1} Hepes (pH 7.5), 50 mmol l^{-1} KCl, 1 mmol l^{-1} dithiothreitol and 0.5 mmol l^{-1} EDTA] and homogenized as above. The homogenate was then centrifuged at 14,500 ***g*** for 5 min at 4°C to pellet cellular material before removing aliquots of the supernatant for each enzymatic assay. GDH (EC 1.4.1.3) activity was measured using previously published methods (e.g. Rubino et al., 2014). The formation rate of glutamate, coupled to the oxidation of NADH in the presence of ADP, was measured with 14 mmol l^{-1} α-ketoglutarate as the substrate (omitted for control). L-type PK (EC 2.7.1.40) activity was measured as previously described (Mommsen et al., 1980). The reaction buffer consisted of imidazole (50 mmol l^{-1}), KCl (100 mmol l^{-1}), $MgCl_2$ (10 mmol l^{-1}), NADH (0.15 mmol l^{-1}), ADP (5 mmol l^{-1}), phosphoenol pyruvate (5.0 mmol l^{-1}; PEP; omitted for control), fructose-1,6 biphosphate (0.1 mmol l^{-1}; FBP) and excess lactic dehydrogenase (∼5 U). LDH (EC 1.1.1.27) was measured in a reaction buffer consisting of imidazole

Journal of Experimental Biology (2019) 222, jeb187484. doi:10.1242/jeb.187484

(50 mmol l^{-1}), NADH (0.15 mmol l^{-1}) and Na^+-pyruvate (0.2 mmol l^{-1}), which was omitted for control. CS (EC 2.3.3.1) was assayed in Tris–HCl buffer (75 mmol l^{-1} pH 8.0) containing DTNB [5,5′-dithio-bis (2-nitrobenzoic acid); 0.1 mmol l^{-1}] and oxaloacetate (OXA; 0.5 mmol l^{-1}) and monitored at 412 nm.

Statistical analysis

All statistical tests were carried out in SigmaStat 3 and plots were constructed in SigmaPlot10 (Systat). Data were first examined for normality and homogeneity of variance before statistical testing. Kinetic data were modeled using SigmaPlot for line of best fit with linear regression or Michaelis–Menten kinetics with single site saturation. Michaelis–Menten kinetics were determined as: $J_{Abs}=J_{Max}\times[X]/([X]+K_M)$, where J_{Abs} is the measured Ca^{2+} influx rate (nmol cm^{-2} min^{-1}), $[X]$ is the Ca^{2+} concentration (in µmol l^{-1}), J_{Max} is the maximal unidirectional flux rate (nmol cm^{-2} min^{-1}) and the K_M value is the Ca concentration (in µmol l^{-1}) providing an uptake rate equal to half J_{Max}. Paired and unpaired Student's *t*-tests were used to determine the difference between unfed and fed transport rates, as well as the average transport rates for each section following La^{3+} application, under asymmetrical conditions. The linear rates of transport following W7 application were compared using an ANCOVA. A one-way repeated-measures ANOVA (treatment as the factor) determined the differences between J_{Max} and K_M values under symmetrical conditions. Likewise, zonation of transport along the proximal–distal axis was examined using a one-way repeated-measures ANOVA (with section as the factor). The impact of inhibitors on the relative ion transport within each section was examined using a two-way repeated-measures ANOVA (inhibitor and caeca portions as factors), whereas the enzyme activities were examined with a two-way repeated-measures ANOVA (with section and treatment as factors). Individual enzyme activities were compared between the two freshwater feeding trials using an unpaired *t*-test. There were no differences found between the two feeding trials ($P>0.05$), thus the results from each were pooled and analyzed together. Unfed NKA activities across sections were compared using a one-way repeated-measures ANOVA, whereas NKA activities across tissue or tissue section and treatment were compared using a two-way repeated-measures ANOVA. All were followed by a Holm–Šidák *post hoc* test. Significance was assessed at $P<0.05$. Values are presented as means ±s.e.m. (*N*=individual preparations from different individuals).

RESULTS

Under asymmetrical conditions, the three caeca sections displayed a net positive flux, indicating absorption into the mucosa (Fig. 1). Unfed animal tissues from the anterior (Fig. 1A), middle (Fig. 1B) or posterior caeca (Fig. 1C) did not display Michaelis–Menten kinetics as the values failed to converge to satisfy the conditions of the model. Instead, there was a combination of sigmoidal or curvilinear absorption at lower Ca^{2+} concentrations followed by a linear increase in absorption with the mucosal bath Ca^{2+} concentrations above 200 µmol l^{-1} for all sections (Fig. 1). Feeding did not alter the general kinetics of transport, with all three sections again failing to meet the conditions for Michaelis–Menten transport; however, the linear transport rates above 200 µmol l^{-1} Ca^{2+} were significantly elevated above the corresponding unfed values for all sections (Fig. 1).

Application of $LaCl_3$ to the serosal and mucosal baths eliminated the correlation between bath Ca^{2+} concentration and mucosal Ca^{2+} transport. The average transport rate for the anterior caeca across all calcium concentrations (9.4±0.4 nmol Ca^{2+} cm^{-2} min^{-1}; *N*=6; Fig. 2A) was similar to that observed in the middle caeca (10.5±0.6 nmol Ca^{2+} cm^{-2} min^{-1}; *N*=6; Fig. 2B) as well as the posterior caeca (9.7±0.7 nmol Ca^{2+} cm^{-2} min^{-1}; *N*=6; Fig. 2C). In

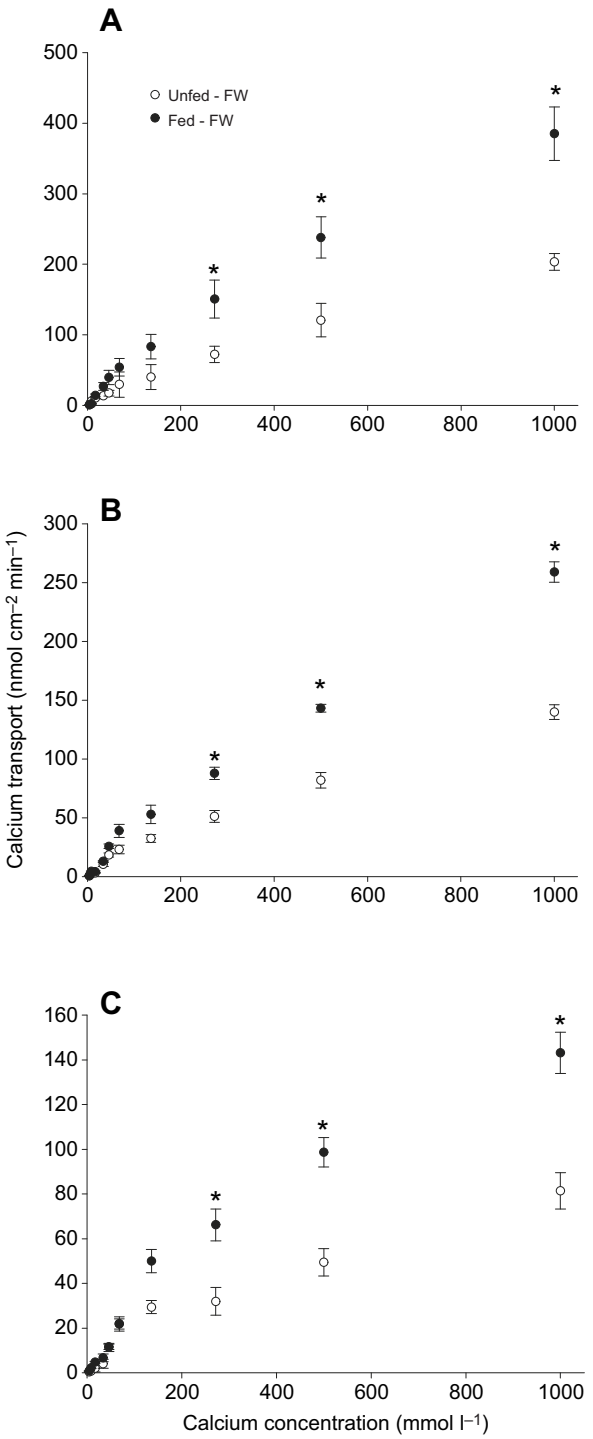

Fig. 1. Ca^{2+} transport (nmol cm^{-2} min^{-1}) in the proximal portion of everted caeca of unfed (open circles) and fed (filled circles) rainbow trout held in freshwater (FW) under asymmetrical conditions. (A) Anterior, (B) middle and (C) posterior caeca. See Table S1 for Ca^{2+} concentrations (µmol l^{-1}) in the serosal and mucosal baths. Kinetics failed to fit Michaelis–Menten parameters (convergence failed). Plotted points represent the means±s.e.m. *N*=6 (individual caeca from different animals). Asterisks represent a statistically significant difference relative to the matched unfed values (paired *t*-test; *$P<0.05$).

Journal of Experimental Biology (2019) 222, jeb187484. doi:10.1242/jeb.187484

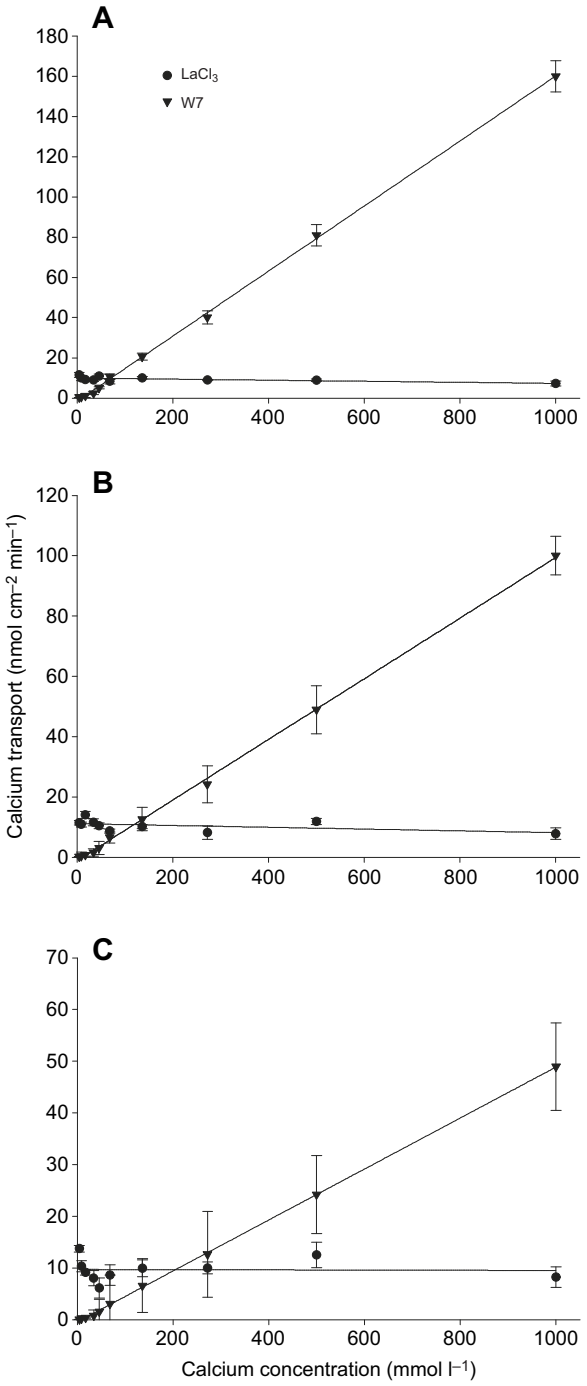

Fig. 2. Effect of $LaCl_3$ (filled circles) and W7 (filled triangles) inhibitors on Ca^{2+} transport (nmol cm^{-2} min^{-1}) in the proximal portion of everted caeca of unfed rainbow trout held in freshwater under asymmetrical conditions. (A) Anterior, (B) middle and (C) posterior caeca. See Table S1 for Ca^{2+} concentrations (μmol l^{-1}) in the serosal and mucosal baths. Linear slopes were obtained for W7 treatments (anterior: y=0.16x–1.53, R^2=0.999; middle: y=0.10x–1.10, R^2=0.999; posterior: y=0.05x–0.41, R^2=0.999) and $LaCl_3$ treatments (anterior: y=–0.0026x+9.93, R^2=0.456; middle: y=–0.0029x+10.11, R^2=0.249; posterior: y=0.0002x+9.75, R^2=0.006). Plotted points represent the means±s.e.m. N=6 (individual caeca from different animals).

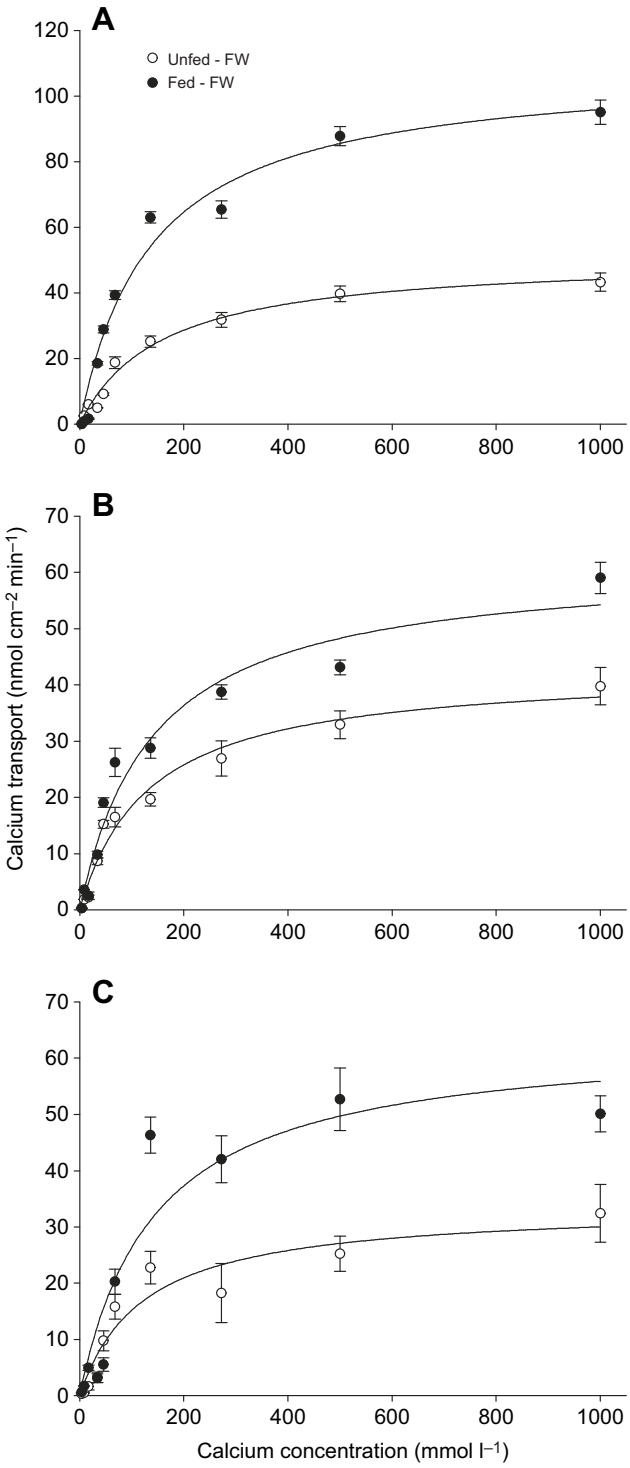

Fig. 3. Ca^{2+} transport (nmol cm^{-2} min^{-1}) in the proximal portion of everted caeca of unfed (open circles) and fed (filled circles) rainbow trout held in freshwater (FW) under symmetrical conditions. (A) Anterior, (B) middle and (C) posterior caeca. See Table S1 for Ca^{2+} concentrations (μmol l^{-1}) in the serosal and mucosal baths. Kinetics successfully fit Michaelis–Menten parameters: $J_{Abs}=J_{Max}\times[X]/([X]+K_M)$. See Results for resulting parameters for each treatment and section. Plotted points represent the means±s.e.m. N=6 (individual caeca from different animals).

contrast, mucosal and serosal W7 application resulted in linear, diffusive transport in all three caeca sections. The slope of the rate of Ca^{2+} transport in the anterior caeca tissue (0.17; Fig. 2A) was 1.7-fold greater than that observed in the middle caeca tissue (0.1; Fig. 2B), which was greater again (2-fold) than the slope detected in the posterior caeca tissue (0.05; Fig. 2C).

Journal of Experimental Biology (2019) 222, jeb187484. doi:10.1242/jeb.187484

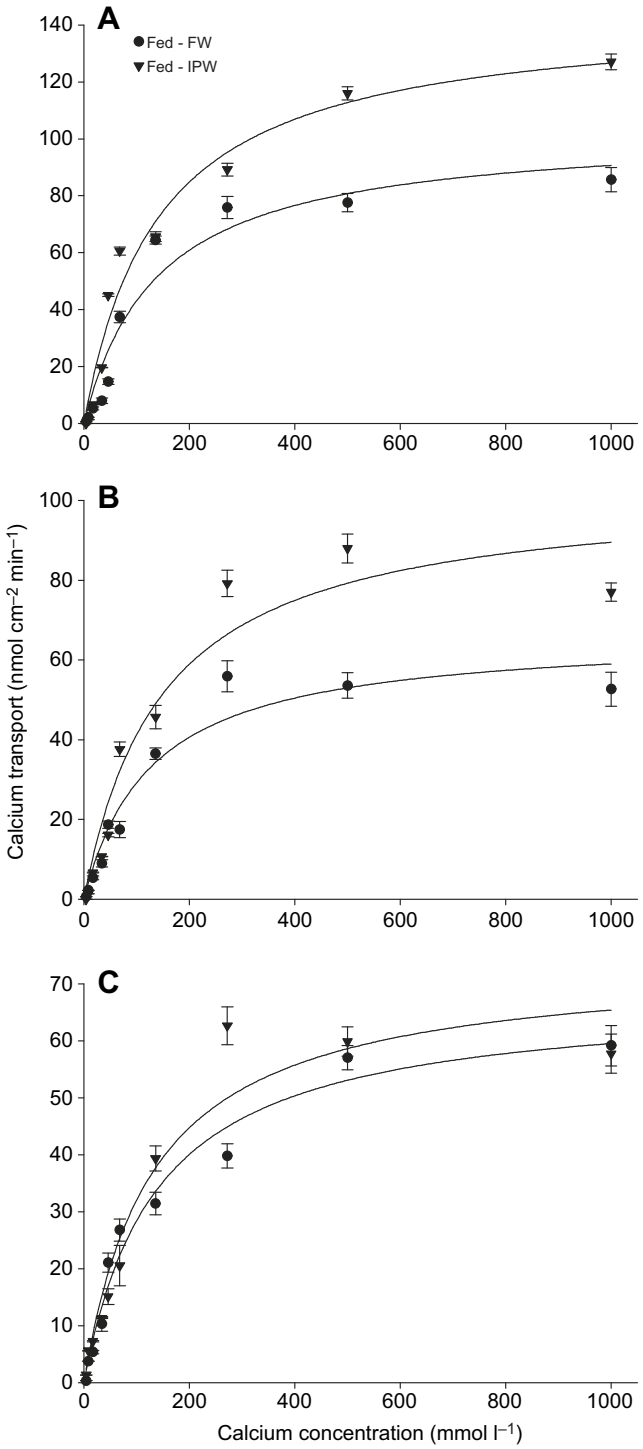

Fig. 4. Ca^{2+} transport (nmol cm^{-2} min^{-1}) in the proximal portion of everted caeca of fed rainbow trout held in freshwater (FW; filled circles) or ion-poor water (IPW; filled triangles) under symmetrical conditions. (A) Anterior, (B) middle and (C) posterior caeca. See Table S1 for Ca^{2+} concentrations (μmol l^{-1}) in the serosal and mucosal baths. Kinetics successfully fit Michaelis–Menten parameters: $J_{Abs}=J_{Max}\times[X]/([X]+K_M)$. See Results for resulting parameters. Plotted points represent the means±s.e.m. N=6 (individual caeca from different animals).

Ca^{2+} transport by the proximal portion of each caeca section displayed typical Michaelis–Menten kinetics under symmetrical Ca^{2+} concentrations, as well as indicating net absorption into the mucosa (Fig. 3). The anterior caeca of unfed fish displayed a J_{Max} of 47.6±2.0 nmol Ca^{2+} cm^{-2} min^{-1} and a K_M of 118.1±2.3 μmol l^{-1} Ca^{2+} (model R^2=0.982; Fig. 3A). Feeding significantly increased the J_{Max} 2.1-fold (101.5±9.3 nmol Ca^{2+} cm^{-2} min^{-1}) and the K_M 1.2-fold to 142.0±3.1 μmol l^{-1} Ca^{2+} (model R^2=0.975; Fig. 3A). The middle caeca of unfed fish exhibited a significantly lower J_{Max} (38.7±3.1 nmol Ca^{2+} cm^{-2} min^{-1}) and similar K_M (113.6±2.3 μmol l^{-1} Ca^{2+}) compared with the anterior caeca (model R^2=0.975; Fig. 3B). Feeding once again increased the J_{Max} (1.6-fold increase; 61.1±5.2 nmol Ca^{2+} cm^{-2} min^{-1}) and K_M 1.2-fold (132.8±2.7 μmol l^{-1} Ca^{2+}), although both the J_{Max} and K_M remained significantly lower than in the anterior caeca of fed fish (model R^2=0.962; Fig. 3B). In the posterior caeca, the J_{Max} for unfed fish was the lowest of all sections (33.4±3.9 nmol Ca^{2+} cm^{-2} min^{-1}), as was the K_M (106.5±4.2 μmol l^{-1} Ca^{2+}; model R^2=0.917; Fig. 3C). Feeding in FW nearly doubled the J_{Max}, significantly elevating the rate to 63.8±9.1 nmol Ca^{2+} cm^{-2} min^{-1}, while the K_M significantly increased 1.4-fold to 142.3±5.8 μmol l^{-1} Ca^{2+} (model R^2=0.897; Fig. 3C). The corresponding values for unfed and fed fish were not statistically different from those from the middle caeca (Fig. 3B); however, the J_{Max} for both unfed and fed fish was significantly lower than the J_{Max} in the anterior caeca, while the K_M for unfed fish alone was lower (Fig. 3A).

Repeating the feeding experiment verified the elevated J_{Max} (103.8±1.5 nmol Ca^{2+} cm^{-2} min^{-1}) and K_M (139.3±3.8 μmol l^{-1} Ca^{2+}) in the anterior caeca (model R^2=0.945; Fig. 4A). Moreover, exposure to IPW further significantly increased the J_{Max} 1.4-fold to 148.4±2.1 nmol Ca^{2+} cm^{-2} min^{-1} and K_M 1.1-fold to 155.7±4.1 μmol l^{-1} Ca^{2+} (model R^2=0.971; Fig. 4A). In comparison, the increased J_{Max} and K_M were also present in a repeated experiment (J_{Max}=66.5±6.3 nmol Ca^{2+} cm^{-2} min^{-1}; K_M=129.0±3.3 μmol l^{-1} Ca^{2+}) for the middle caeca obtained from fed animals (model R^2=0.950; Fig. 4B). Additionally, IPW exposure similarly increased J_{Max} 1.4-fold (101.9±1.4 nmol Ca^{2+} cm^{-2} min^{-1}) and K_M 1.1-fold (149.1±2.3 μmol l^{-1} Ca^{2+}; model R^2=0.942; Fig. 4B). J_{Max} observed in the middle caeca tissue once again remained significantly lower than in the anterior caeca, while the K_M was not significantly different (Fig. 4B). Finally, repeating the feeding experiment once again resulted in similar transport characteristics of fed tissue (J_{Max}=67.8±4.3 nmol Ca^{2+} cm^{-2} min^{-1}, K_M=137.8±2.5 μmol l^{-1} Ca^{2+}) in the posterior caeca (model R^2=0.976; Fig. 4C). However, unlike the middle

Table 1. Zonation of Ca^{2+} transport parameters J_{Max} (nmol cm^{-2} min^{-1}) and K_M (μmol l^{-1}) from proximal (close to intestine proper) to distal (tip of the caeca) within individual caeca obtained from three regions of the anterior intestine of unfed freshwater rainbow trout

		Kinetic parameters	
Caeca section	Portion of caeca	J_{Max}	K_M
Anterior	Proximal	43.7±5.6[a]	120.4±5.1[a]
	Mid	30.2±3.1[b]	116.1±4.7[a]
	Distal	15.6±1.9[c,d]	110.8±6.0[a,b]
Middle	Proximal	31.2±3.9[b]	112.2±5.3[a]
	Distal	12.0±5.2[c,d]	110.3±5.6[a,b]
Posterior	Proximal	27.4±2.7[b]	101.6±3.8[b]
	Distal	10.8±3.5[d]	102.9±4.2[b]

Values within a column sharing a letter are not significantly different (P>0.05) according to a one-way repeated-measures ANOVA (portion of caeca as the factor) followed by a Holm–Šidák *post hoc* test. N=6 (individual caeca from different animals). Michaelis–Menten kinetic parameters were obtained from transport versus concentration graphs as shown in Fig. 3 using symmetrical conditions.

Journal of Experimental Biology (2019) 222, jeb187484. doi:10.1242/jeb.187484

Table 2. Zonation of Ca^{2+} transport inhibition (% of control) from proximal (close to intestine proper) to distal (tip of the caeca) within individual caeca from three regions of the anterior intestine obtained from unfed freshwater rainbow trout

		% Inhibition (500 μmol l^{-1} Ca^{2+})			
Caeca section	Portion of caeca	Control	Ouabain	La^{3+}	W7
Anterior	Proximal	100±5	33±7[a]	61±6[b]	15±3[c]
	Mid	100±7	32±6[a]	76±4[b]	9±4[c]
	Distal	100±4	36±3[a]	70±5[b]	12±3[c]
Middle	Proximal	100±6	31±5[a]	67±3[b]	15±2[c]
	Distal	100±3	29±3[a]	69±3[b]	13±4[c]
Posterior	Proximal	100±5	39±6[a]	70±6[b]	10±3[c]
	Distal	100±8	31±3[a]	66±5[b]	12±2[c]

Different letters within a row indicate a significant difference from control (P<0.05) according to a two-way repeated-measures ANOVA (with portion and inhibitor as factors) followed by a Holm–Šidák *post hoc* test. N=6 (individual caeca from different animals). Control values were set to 100%. Inhibitors were tested at a single, symmetrical bath concentration (500 μmol l^{-1} Ca^{2+}). Ouabain (100 μmol l^{-1}), $LaCl_3$ (200 μmol l^{-1}) and W7 (1 μmol l^{-1}) were added to both the mucosal and serosal baths.

and anterior caeca, exposure to IPW did not further alter the J_{Max} (77.1±5.9 nmol Ca^{2+} cm^{-2} min^{-1}) or the K_M (143.4±3.3 μmol l^{-1} Ca^{2+}; model R^2=0.948; Fig. 4C). The K_M of the IPW posterior caeca was significantly lower than that in the anterior caeca, while the J_{Max} of the IPW posterior caeca was lower than both the middle and anterior caeca.

There was further zonation within each caeca section under symmetrical conditions. Moving from the proximal portion adjacent to the intestine proper towards the distal tip of each caeca section, there was a significant decrease in J_{Max}, while K_M was unaffected in unfed animal tissues (Table 1). Once again, there was a significant reduction in J_{Max} and K_M from the anterior to posterior sections, although this trend was only significant in the proximal portions; the distal portions showed no zonation along the anterior–posterior axis (Table 1).

When analyzing the impact of inhibitors on Ca^{2+} transport using a two-way repeated-measures ANOVA (inhibitor and portion of caeca as factors), there was no significant interaction (P=0.108) nor was there an effect of portion of caeca (P=0.422), whereas there was a significant effect of inhibitor application (P<0.001). Under symmetrical conditions, tissue exposed to ouabain significantly decreased Ca^{2+} transport across all sections and portions of the caeca to values ∼33% lower than those of the control (Table 2). Similarly, application of La^{3+} to the mucosal and serosal surfaces significantly reduced Ca^{2+} transport similarly across all three caeca sections and portions, decreasing transport by approximately 68% compared with control values (Table 2). Finally, application of W7 likewise significantly diminished Ca^{2+} transport consistently across portions and sections; however, transport was reduced by the greatest proportion to ∼12% of control values (Table 2).

Statistical analysis revealed a lack of significance in caeca portion (P=0.892) and a lack of interaction between caeca portion and treatment (P=0.708), allowing for direct interpretation of the significant effect (P<0.01) of treatment on GDH activity (Table 3). There was a significant increase in GDH activity in the IPW treatment over the unfed and fed treatments; however, there was not a significant difference between unfed and fed animals. PK activity likewise showed a significant effect of treatment (P<0.01), whereas caeca portion did not influence activity rates (P=0.152) and there was a lack of interaction between the two factors (P=0.107). As with GDH, IPW exposure elevated PK activity rates over those observed in fed and unfed animals; however, in contrast, there was also a significant increase in fed animals when compared with unfed animals (Table 3). LDH activity was significantly reduced below unfed values in both the fed and IPW-exposed animals (P<0.01); however, fed and IPW animals were not different (Table 3). There was again a lack of significant effect of caeca portion for LDH activity (P=0.099) and a lack of interaction between factors (P=0.422). As with PK, feeding significantly elevated CS levels above those observed in unfed animals, and IPW exposure significantly elevated activity further (P<0.05; Table 3). In contrast, however, there was a significant effect of section (P=0.02), with anterior portions displaying elevated CS activity over posterior portions, while no consistent differences appeared on the proximal–distal axis (Table 3). A lack of interaction between the treatment and portion of caeca factors (P=0.072) allowed for direct interpretation of these effects. Finally, NKA activity in unfed animal tissues showed a strong significant effect of section (anterior to posterior) as well as portion (proximal to distal), with the anterior

Table 3. Impact of feeding and ion-poor water (IPW) exposure on enzyme activity and zonation within individual caeca from proximal (close to intestine proper) to distal (tip of the caeca) in three regions of the anterior intestine obtained from rainbow trout

		Anterior caeca		Middle caeca		Posterior caeca	
Enzyme	Treatment	Proximal	Distal	Proximal	Distal	Proximal	Distal
Glutamate dehydrogenase	Unfed	5.7±0.7[a,b]	4.5±2.2[a]	4.9±0.4[a]	4.4±1.0[a]	3.9±1.3[a]	4.8±1.3[a]
	Fed	4.7±0.9[a]	5.6±0.7[a]	5.1±0.3[a]	4.8±1.1[a]	5.0±0.5[a]	4.9±1.5[a]
	IPW	7.8±0.5[b]	7.2±1.0[a]	8.1±0.7[b]	6.7±2.9[a]	7.7±0.5[b]	6.7±0.9[a]
Pyruvate kinase	Unfed	5.2±0.6[a]	6.1±1.8[a]	5.9±0.7[a]	4.6±1.8[a]	5.0±1.3[a]	7.1±2.6[a]
	Fed	18.6±2.1[b]	22.2±4.3[b]	15.5±1.9[b]	14.6±3.6[b]	13.6±2.9[b]	19.2±3.2[b]
	IPW	33.3±3.6[c]	29.7±3.6[c]	27.3±4.5[c]	24.5±2.1[c]	39.5±8.1[c]	32.6±2.9[c]
Lactate dehydrogenase	Unfed	15.7±1.5[a]	13.8±2.6[a,c]	12.6±1.3[a,c]	12.0±2.2[a,c]	13.9±1.7[a]	14.8±2.4[a]
	Fed	7.9±1.6[b]	8.2±1.3[b]	6.5±1.1[a,b]	4.7±2.0[b]	5.6±0.9[b]	7.5±1.7[b]
	IPW	9.9±1.8[b,c]	10.3±2.6[b,c]	7.0±1.1[b]	9.2±2.8[b,c]	7.9±1.4[b]	6.9±1.2[b]
Citrate synthase	Unfed	7.12±0.67[a]	8.9±1.1[a]	6.5±0.2[a]	6.4±1.5[a,d]	6.6±0.8[a,d]	5.3±0.9[d]
	Fed	18.3±1.3[b]	15.9±1.1[b,e]	13.8±1.5[e]	17.8±2.0[b]	13.5±2.3[e]	13.7±1.9[e]
	IPW	27.7±3.0[c]	24.0±2.4[c,f]	21.7±0.7[f]	26.8±1.8[c]	18.5±1.1[b]	12.7±2.8[e]
Na^+/K^+-ATPase	Unfed	5.6±0.9[a]	3.4±0.7[b,c]	4.2±0.6[a,b]	2.5±0.5[c]	3.9±0.6[b]	2.1±0.3[c]

Values within a metabolite or enzyme sharing a letter are not significantly different (P>0.05) according to a two-way ANOVA (treatment and location as factors) followed by a Holm–Šidák *post hoc* test, except Na^+/K^+-ATPase (NKA). NKA values sharing letters are not significantly different (P>0.05) according to a one-way ANOVA (section as the factor) followed by a Holm–Šidák *post hoc* test. N=8 (pooled caeca from different animals). Maximal enzyme activity rates are measured in IU g^{-1} protein at 25°C or μmol ADP mg^{-1} protein h^{-1} (NKA only). NKA fed and IPW values are shown in Fig. 5.

Journal of Experimental Biology (2019) 222, jeb187484. doi:10.1242/jeb.187484

proximal area exhibiting the highest activity rates and the posterior distal area the lowest (Table 3).

Further exploration of NKA activity rates confirmed a gradient along the anterior to posterior axis, with anterior caeca displaying the highest NKA activity rates and the posterior caeca the lowest (Fig. 5A). The anterior intestine proper presented NKA activity rates that were similar to those of the middle and posterior caeca (average across sections 3.5±0.4 µmol ADP mg^{-1} protein h^{-1}; N=8; Fig. 5A). Feeding increased NKA activity rates in the anterior intestine proper, anterior caeca, middle caeca and posterior caeca (Fig. 5A). IPW exposure likewise increased NKA activity rates above fed values in the anterior intestine proper and anterior caeca; however, the middle and posterior caeca were unaffected (Fig. 5A). In contrast, feeding and IPW exposure did not elevate kidney NKA rates above those observed in unfed animals (Fig. 5B), whereas feeding elevated branchial NKA rates above unfed rates, and IPW exposure further elevated rates above feeding (Fig. 5B). There was no interaction between factors (P=0.791).

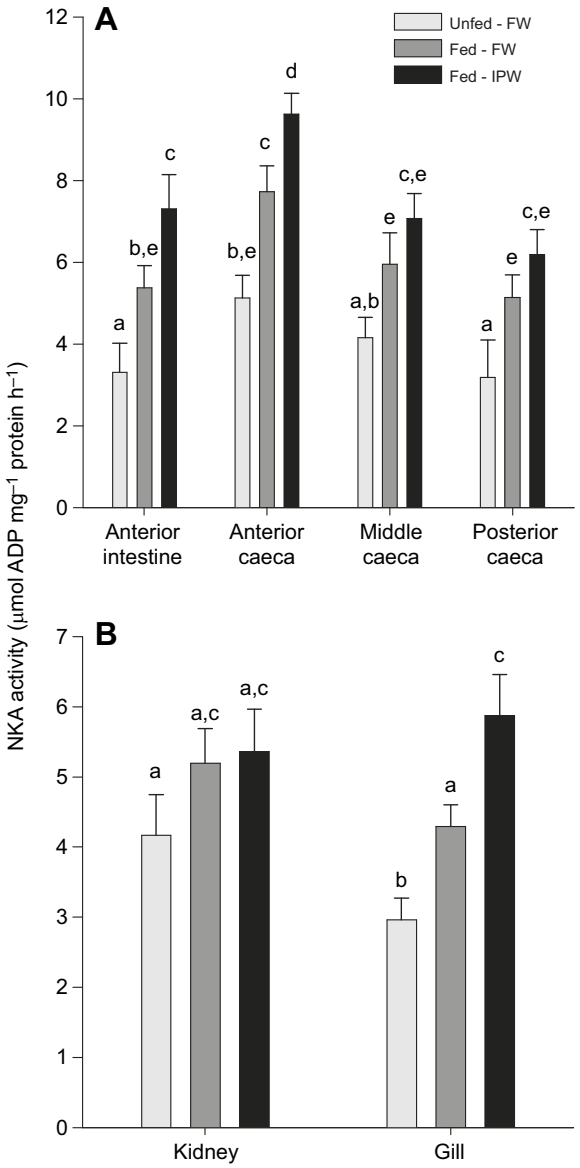

Fig. 5. Na^+/K^+-ATPase (NKA) activity (µmol ADP mg^{-1} protein h^{-1}) in response to water type and feeding status. (A) Intestine and (B) kidney and gill. White bars are unfed fish acclimated to freshwater (FW). Dark gray bars are fed fish acclimated to freshwater. Black bars are fed fish acclimated to ion-poor water (IPW) for 24 h. Plotted points represent the means+s.e.m. N=8 (pooled caeca from different animals). Within each panel, bars sharing letters are not significantly different (P>0.05) according to a two-way repeated-measures ANOVA followed by a Holm–Šidák *post hoc* test. Statistical testing revealed a significant impact of tissue and treatment, but there was no interaction between parameters for any tissues (P>0.05).

DISCUSSION

Ca^{2+} transport in the intestine displayed elements of both paracellular and transcellular transport. Under asymmetrical conditions, all three sections of the caeca showed diffusive absorption at higher Ca^{2+} concentrations (Fig. 1), indicative of paracellular movement. In addition, under symmetrical conditions, all three sections have shown typical transport kinetics of transcellular absorption (Figs 2 and 3). Based on these observations and previous research (Perry and Flik, 1988; Flik and Verbost, 1993; Klaren et al., 1993; Flik et al., 1996), we propose the following transport model within the enterocytes of the caeca (Fig. 6). Here, Ca^{2+} enters the cell through an apical channel and is extruded across the basolateral membrane by a plasma membrane Ca^{2+}-ATPase (PMCA) and/or an Na^+-Ca^{2+} exchanger (NCX), which is dependent on the NKA to create a favorable Na^+ gradient (Fig. 6). Furthermore, paracellular diffusion likely occurs between the cells through the intracellular tight junctions (Fig. 6). Inhibition by ouabain supports the role of the NKA in the observed Ca^{2+} transport (Table 2), while W7 inhibition supports the role of a PMCA (Garrahan, 2018). La^{3+} inhibition of transport (Fig. 2, Table 2) suggests a blockade of paracellular diffusion as well as transcellular transport, possibly through an epithelial Ca^{2+} channel (Verbost et al., 1987; Perry and Flik, 1988; Hogstrand et al., 1995, 1996; Fig. 6). Low to negligible expression of the epithelial Ca^{2+} channel (ECaC) was detected in the intestine of rainbow trout (Shahsavarani, 2006), suggesting an alternative channel (Larsson et al., 1998). Paracellular inhibition of transport may be accounted for by the preference of claudin-2 (a tight-junction forming protein) for La^{3+} (Yu et al., 2010). Interestingly, Abaurrea-Equisoaín and Ostos-Garrido (1996) suggested two ion-transporting cell types in the caeca of rainbow trout. The role of distinct cell types in the caeca is unclear, but examination of the ion transport model of the rainbow trout gill suggests that the cells may individually contribute specific ion-transport pathways (Galvez et al., 2002; Hwang et al., 2011).

Feeding increased transport rates in all sections, with the largest effect present in the anterior caeca (Fig. 6), through increased paracellular diffusion (Fig. 1) as well as increased transcellular capacity and decreased specificity (Fig. 3). Increases in paracellular transport rates suggest an increase in tissue permeability, likely via alterations in the tight junctions between cells. Direct evidence that digesting a meal alters the permeability of the intestine is lacking in fish; however, increased water absorption in the intestine of fed FW fish (Bucking and Wood, 2006b) provides indirect evidence of increased permeability. Should this be occurring, tight-junction proteins such as those from the occludin and claudin family would likely reveal alterations in expression and/or function during feeding. In contrast, the increase in transcellular transport during digestion may have been accomplished by increasing the number of high-capacity, low-affinity transporters (i.e. NCX; Fig. 6), and/or increasing the activity of said transporters through post-translational modifications. This is the first evidence of such compensation during digestion; however, this has been observed in response to environmental manipulations (Schoenmakers et al., 1993). The NCX predominated over the PMCA, which is a comparatively low-capacity, high-affinity transporter (e.g. Blaustein and Lederer,

Journal of Experimental Biology (2019) 222, jeb187484. doi:10.1242/jeb.187484

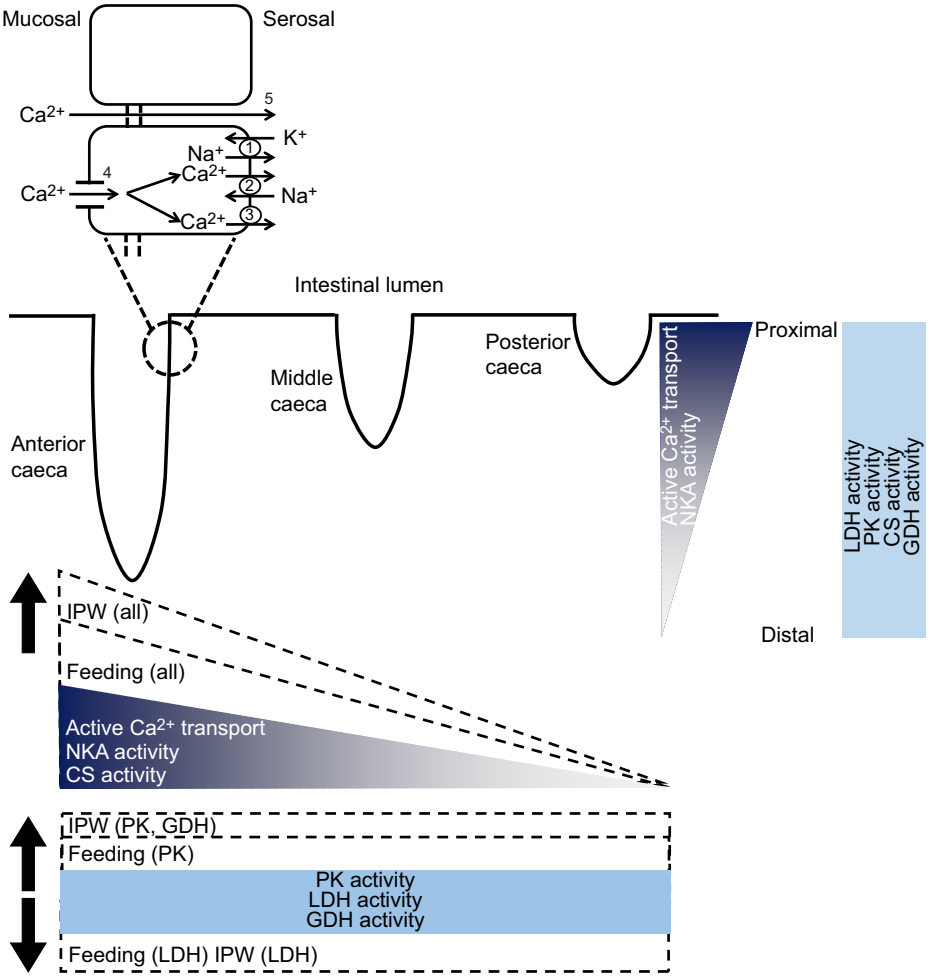

Fig. 6. Summary and model of Ca^{2+} transport and enzyme activity in the proximal and distal portions of the caeca along the anterior–posterior axis of the anterior intestine. For the Ca^{2+} transport model, mucosal to serosal movement is shown to depend on: (1) Na^+/K^+-ATPase (NKA); (2) Na^+-Ca^{2+} exchanger (NCX); (3) Ca^{2+}-ATPase (PMCA); (4) Ca^{2+} channel; and (5) paracellular transport. Ca^{2+} transport, NKA activity and citrate synthase (CS) activity all show a gradient along the anterior–posterior axis amongst caeca (indicated by thickness and color of bar), whereas only Ca^{2+} transport and NKA activity show a gradient along the proximal–distal axis within each caecum. Metabolic enzymes [pyruvate kinase (PK), lactate dehydrogenase (LDH) and glutamate dehydrogenase (GDH)] show no zonation (indicated by gray uniform bar). The impacts of feeding and IPW exposure are shown as increases or decreases over unfed control values (indicated by dashed areas and arrows).

1999), even in the unfed tilapia intestine (Flik et al., 1996). This may indicate species-specific regulation of intestinal Ca^{2+} transport.

Exposure to IPW further increased ion transport rates above those seen during digestion. Again, this occurred primarily through an increased J_{Max} and slightly increased K_M, suggesting a similar increase in transporter capacity either through an increase in number and/or a prevalence of the NCX (Figs 3 and 6). In contrast to feeding, this response was not evident in the posterior portions of the caeca (Fig. 4). The opposite occurs during a FW–SW transfer, when demand for Ca^{2+} uptake is reduced, as activities of the PMCA and the NCX decrease; suggested to be an adjustment of Ca^{2+} carrier densities in the basolateral plasma membrane (Schoenmakers et al., 1993). Interestingly, the tubular networks found within the suspected ion-transporting cells are more developed in SW-exposed fish (Giffard-Mena et al., 2006), suggesting an environmental control over caeca morphology and subsequent physiological role. This may reflect intestinal water and salt transport required by SW teleost fish whereby active transport of solutes, sodium and chloride in particular as well as the excretion of bicarbonate (e.g. Ando, 1988; Usher et al., 1991; Wilson et al., 1996; Grosell et al., 2009), creates an osmotic drag to pull water across the intestine (e.g. reviewed by Whittamore, 2012). Combined with this is the precipitation of bicarbonate with calcium, lowering the osmotic pressure of the fluid in the intestine, aiding water uptake into the plasma (Wilson et al., 1996) and resulting in a reduced need for Ca^{2+} absorption. Feeding was an important control for the IPW exposure, as animals faced a risk of mortality if food was withheld during exposure (based on previous laboratory observations). It is possible that exposure to lowered salinity is compensated for directly through digestion, by providing either ions and/or energy. Indeed, the importance of dietary ions has been shown with decreasing salinity in numerous species (Wood and Laurent, 2003; Scott et al., 2006; Marshall and Grosell, 2006).

It is important to note that the observed K_M values (110 µmol l^{-1} in the present study) vary from published values from other fish species (e.g. 0.19–2.3 µmol l^{-1} in the tilapia intestine). Furthermore, the K_M for the PMCA is roughly 0.3 µmol l^{-1} in mammalian studies (Carafoli, 1992), whereas NCX is approximately 10-fold less (approximately 3 µmol l^{-1}; Blaustein and Lederer, 1999). In general, we underestimated the K_M by ∼50-fold; however, other studies have over/underestimated these values using traditional radioisotopes by more than 1000-fold (Klinck et al., 2012). This strongly suggests that while using SIET to measure ion transport, relative changes in magnitude with treatment are indicative of effect, whereas absolute values may not be representative. Remarkably, the J_{Max} of Ca^{2+} uptake into the mucus binding compartment of the anterior intestine proper of freshwater rainbow trout was ∼8 nmol min^{-1} cm^{-2} (Klinck et al., 2012), roughly similar to the average uptake rate during La^{3+} exposure (Fig. 2), suggesting this may reflect background absorption into the mucous and/or bacteria.

Feeding and IPW exposure increased NKA activity in parallel with ion transport (Fig. 5), possibly aiding increased Ca^{2+} absorption (Fig. 6). Increased enterocyte NKA activity during digestion has been previously observed (e.g. Turner and Bucking,

2017) and likely supports increased ion transport associated with digestion (Bucking and Wood, 2006a). The few studies examining the transition from FW to IPW have revealed physiological changes that mirror those exhibited by euryhaline fishes during SW–FW transfer, i.e. lowered serum osmolality and circulating ion levels, as well as increased circulating glucose and intestinal NKA activity (Chasiotis et al., 2009). Although abrupt transfer has not been examined in the gut, longer-term acclimation to IPW also showed a variable decrease in intestinal occludin expression (Chasiotis et al., 2009), suggesting both paracellular and transcellular Ca^{2+} absorption increases during IPW exposure (Fig. 6). Scott et al. (2006) proposed that increased ion uptake across the intestine with decreasing salinity was driven by paracellular transport, not transcellular transport. Interestingly, long-term acclimation (28 days) of goldfish suggested that following an initial increase in paracellular transport, this is decreased and followed by an increase in transcellular transport (Chasiotis et al., 2009).

Feeding and IPW exposure altered enzymatic activities in a manner paralleling ATP demand through increased NKA activity (Table 3). In particular, CS, a key enzyme in the Krebs cycle and an indicator of mitochondria function and hence ATP production, mirrored NKA activity and ion transport patterns (Fig. 6). Traditionally, the effect of salinity changes on metabolic pathways has been examined in the liver (e.g. PK activity increases ∼1.5-fold, LDH increases 2- to 3-fold; Soengas et al., 1995a; Vijayan et al., 1996). Alterations in hepatic metabolism likely act to provide glucose and lactate for oxidation in the gill (Mommsen, 1984; Perry and Walsh, 1989), supporting the increased energy requirement of the gills as a result of altered ion transporter activity (e.g. Vijayan et al., 1996; Chang et al., 2007). In fact, during SW adaptation, the gills, kidney and intestine can increase total energy consumption (e.g. Evans, 1984; Soengas et al., 1995b); however, they lack extensive energetic reserves, such as glycogen or lipids (Perry and Walsh, 1989; Soengas et al., 1995b), which are rapidly depleted during acclimation (Chang et al., 2007). It is possible that the liver is not the only organ that alters metabolic pathways, as numerous reaction pathways were enhanced in IPW-acclimated fish (Table 3). When fed, SW transfer resulted in no apparent increase in substrate mobilization from the liver (Vijayan et al., 1996). Perhaps the intestine was supplying more substrates in the plasma, avoiding an increase in energy mobilization from the liver. The intestine of rainbow trout is notable for its capacity to store glucose as glycogen in the muscle layers, to oxidize glucose into lactate, and to regulate its own glucose homeostasis and glycolytic capacity (Polakof et al., 2010).

There was clear zonation in ion transport and NKA activity, along both the proximal–distal (Table 1) and anterior–posterior axes (Figs 3 and 6). Anterior–posterior zonation was also seen with CS activity (Figs 5 and 6); however, the other metabolic enzymes examined did not display zonation (Table 3; Fig. 6). The proximal–distal zonation was expected based on indications of cell-type zonation, with absorptive (Anderson, 1986) and possible ion-transporting cells (Abaurrea-Equisoaín and Ostos-Garrido, 1996). However, zonation along the anterior–posterior axis was unexpected (Williams and Nickol, 1989). Broad zonation along the anterior–posterior axis of the entire gut has been observed. Generally, the anterior intestines of teleosts display histological features that suggest lipid and amino acid absorption (Sire et al., 1981; Ostos Garrido et al., 1993), whereas the posterior intestine demonstrates macromolecule absorption via pinocytosis (Ezeasor and Stokoe, 1981; Anderson, 1986; Abaurrea et al., 1993). For example, intestinal nutrient transport showed zonation along the gut of coho salmon (proline uptake: caeca>>anterior intestine>posterior intestine; Collie, 1985), driven by an increased J_{Max} and similar K_M, suggesting an increased number of transporters as opposed to an isoform gradient. The fine-scale zonation in ion transport within the caeca themselves is a novel observation and the implication requires further research. It is interesting to observe that the anterior intestine proper had slightly lower NKA activities compared with the anterior caeca (Fig. 5A), despite the well-known role in nutrient absorption and digestion. This may be a result of increased muscle thickness around the intestine proper diluting the detected activity of NKA.

We have used a novel technique to establish the kinetics of Ca^{2+} transport in the caeca of rainbow trout, as well as responses to pharmacological inhibitors and environmental manipulation and digestion. Ca^{2+} transport in the caeca matches existing transport models with both paracellular and transcellular pathways. We have discovered zonation in this function, with proximal and anterior portions displaying the highest level of activity, coinciding with ultrastructural evidence. Ion transport patterns correlated with NKA and CS activity, suggesting an increase in ATP use and production. Increased carbohydrate and amino acid metabolism may have provided the ATP; however, zonation was not apparent. This supports the hypothesis that the diet contributes a substantial amount of ions required to maintain homeostasis, and during IPW exposure the contribution may further increase to compensate for a limited ability to acquire ions from the surrounding environment. Overall, our results suggest that the caeca of trout are heterogeneous appendages, with functional zones dedicated to active ion transport supported by energy production through local enzyme activity.

Acknowledgements
Thanks are given to A. Donini for his support and access to the SIET system. Sampling help from D. Ahkmen and H. Groser was appreciated. We thank the reviewers for their helpful comments, and appreciate their efforts.

Competing interests
The authors declare no competing or financial interests.

Author contributions
Conceptualization: M.W., D.B., C.B.; Methodology: M.W., D.B., C.B.; Formal analysis: M.W., D.B., C.B.; Investigation: M.W., D.B.; Writing - original draft: C.B.; Writing - review & editing: M.W., D.B., C.B.; Supervision: C.B.; Funding acquisition: C.B.

Funding
This work was supported by a Natural Sciences and Engineering Research Council of Canada Discovery Grant to C.B. as well as a Canada Foundation for Innovation John R. Evans Leaders Fund (JELF) grant.

Supplementary information
Supplementary information available online at
http://jeb.biologists.org/lookup/doi/10.1242/jeb.187484.supplemental

References
Abaurrea, M. A., Nuñez, M. I. and Ostos, M. V. (1993). Ultrastructural study of the distal part of the intestine of *Oncorhynchus mykiss*. Absorption of dietary protein. *Micron* **24**, 445-450.
Abaurrea-Equisoaín, M. A. and Ostos-Garrido, M. V. (1996). Enterocytes in the anterior intestine of *Oncorhynchus mykiss*: cytological characteristics related to osmoregulation. *Aquaculture* **139**, 109-116.
Anderson, T. A. (1986). Histological and cytological structure of the gastrointestinal tract of the luderick, *Girella tricuspidata* (Pisces, Kyphosidae), in relation to diet. *J. Morphol.* **190**, 109-119.
Ando, B. Y. M. (1988). Amino acid transport in eel intestine. *J. Exp. Biol.* **106**, 93-106.
Bauermeister, A. E. M., Pirie, B. J. S. and Sargent J. R. (1979). An electron microscopic study of lipid absorption in the pyloric caeca of rainbow trout (*Salmo gairdnerii*) fed wax ester-rich zooplankton. *Cell Tiss. Res.* **200**, 475-486.
Blaustein, M. P. and Lederer, W. J. (1999). Sodium calcium exchange: its physiological implications. *Physiol. Rev.* **79**, 763-854.

Bogé, G., Lopez, L. and Pérès, G. (1988). An *in vivo* study of the role of pyloric caeca in water absorption in rainbow trout (*Salmo gairdneri*). *Comp. Biochem. Physiol. Part A Physiol.* **91**, 9-13.
Brijs, J., Axelsson, M., Grans, A., Pichaud, N., Olsson, C. and Sandblom, E. (2015). Increased gastrointestinal blood flow: An essential circulatory modification for euryhaline rainbow trout (*Oncorhynchus mykiss*) migrating to sea. *Sci. Reports.* **5**, 10430.
Bucking, C. and Wood, C. M. (2006a). Gastrointestinal processing of Na^+, Cl^-, and K^+ during digestion: implications for homeostatic balance in freshwater rainbow trout. *Am. J. Physiol. Integr. Comp. Physiol.* **291**, R1764-R1772.
Bucking, C. and Wood, C. M. (2006b). Water dynamics in the digestive tract of the freshwater rainbow trout during the processing of a single meal. *J. Exp. Biol.* **209**, 1883-1893.
Bucking, C. and Wood, C. (2012). Digestion of a single meal affects gene expression of ion and ammonia transporters and glutamine synthetase activity in the gastrointestinal tract of freshwater rainbow trout. *J. Comp. Physiol. B* **182**, 314-350.
Bucking, C., LeMoine, C. M. R., Craig, P. M. and Walsh, P. J. (2013). Nitrogen metabolism of the intestine during digestion in a teleost fish, the plainfin midshipman (*Porichthys notatus*). *J. Exp. Biol.* **216**, 2821-2832.
Buddington, R. K. and Diamond, J. M. (1987). Pyloric ceca of fish: a "new" absorptive organ. *Am. J. Physiol.* **252**, G65-G76.
Burnstock, G. (1959). The morphology of the gut of the brown trout (*Salmo trutta*). *Q. J. Microsc. Sci.* **3**, 183-198.
Carafoli, E. (1992). The Ca^{2+} pump of the plasma membrane. *J. Biol. Chem.* **267**, 2115-2118.
Chang, J. C.-H., Wu, S.-M., Tseng, Y.-C., Lee, Y.-C., Baba, O. and Hwang, P.-P. (2007). Regulation of glycogen metabolism in gills and liver of the euryhaline tilapia (*Oreochromis mossambicus*) during acclimation to seawater. *J. Exp. Biol.* **210**, 3494-3504.
Chasiotis, H., Effendi, J. C. and Kelly, S. P. (2009). Occludin expression in goldfish held in ion-poor water. *J. Comp. Physiol. B.* **179**, 145-154.
Chen, B. N., Qin, J. G., Kumar, M. S., Hutchinson, W. and Clarke, S. (2006). Ontogenetic development of the digestive system in yellowtail kingfish *Seriola lalandi* larvae. *Aquaculture* **256**, 489-501.
Chew, S. F., Tng, Y. Y. M., Wee, N. L. J., Tok, C. Y., Wilson, J. M. and Ip, Y. K. (2010). Intestinal osmoregulatory acclimation and nitrogen metabolism in juveniles of the freshwater marble goby exposed to seawater. *J. Comp. Physiol. B Biochem. Syst. Environ. Physiol.* **180**, 511-520.
Collie, N. L. (1985). Intestinal nutrient transport in coho salmon (*Oncorhynchus kisutch*) and the effects of development, starvation, and seawater adaptation. *J. Comp. Physiol. B* **156**, 163-174.
Edwards, S. and Marshall, W. (2012). Principles and patterns of osmoregulation and euryhalinity in fishes. In *Fish Physiology*, Vol. 32 (ed. S. McCormick, A. Farrell and C. Brauner), pp. 1-44. Academic Press.
Evans, D. (1984). The roles of gill permeability and transport mechanisms in euryhalinity. In *Fish Physiology* (ed. W. S. Hoar and D. J. Randall), pp. 239-279.
Evans, D. H., Piermarini, P. M. and Choe, K. P. (2005). The multifunctional fish gill: dominant site of gas exchange, osmoregulation, acid-base regulation, and excretion of nitrogenous waste. *Physiol. Rev.* **85**, 97-177.
Ezeasor, D. N. and Stokoe, W. M. (1981). Light and electron microscopic studies on the absorptive cells of the intestine, caeca and rectum of the adult rainbow trout, *Salmo gairdneri*, Rich. *J. Fish Biol.* **18**, 527-544.
Faulk, C. K., Benninghoff, A. D. and Holt, G. J. (2007). Ontogeny of the gastrointestinal tract and selected digestive enzymes in cobia *Rachycentron canadum* (L.). *J. Fish Biol.* **70**, 567-583.
Flik, G. and Verbost, P. M. (1993). Calcium transport in fish gills and intestine. *J. Exp. Biol.* **184**, 17-29.
Flik, G., Klaren, P. H. M., Schoenmakers, T. J. M. and Bijvelds, M. J. C. (1996). Cellular calcium transport in fish: unique and universal mechanisms. *Physiol. Zool.* **69**, 403-417.
Galvez, F., Reid, S. D., Hawkings, G. and Goss, G. G. (2002). Isolation and characterization of mitochondria-rich cell types from the gill of freshwater rainbow trout. *Am. J. Physiol. Integr. Comp. Physiol.* **282**, R658-R668.
Garrahan, P. (2018). Inhibitors of the Ca^{2+} pump. In *The Ca^{2+} Pump of Plasma Membranes* (ed. A. Rega and P. Garrahan), pp. 153-164. Boca Raton: CRC Press.
Giffard-Mena, I., Charmantier, G., Grousset, E., Aujoulat, F. and Castille, R. (2006). Digestive tract ontogeny of *Dicentrarchus labrax*: implication in osmoregulation. *Dev. Growth Differ.* **48**, 139-151.
Grosell, M., Gilmour, K. and Perry, S. (2007). Intestinal carbonic anhydrase, bicarbonate, and proton carriers play a role in the acclimation of rainbow trout to seawater. *Am. J. Physiol. Integr. Comp. Physiol.* **293**, R2099-R2111.
Grosell, M., Genz, J., Taylor, J. R., Perry, S. F. and Gilmour, K. M. (2009). The involvement of H^+-ATPase and carbonic anhydrase in intestinal HCO_3^- secretion in seawater-acclimated rainbow trout. *J. Exp. Biol.* **212**, 1940-1948.
Hogstrand, C., Reid, S. and Wood, C. (1995). Ca^{2+} versus Zn^{2+} transport in the gills of freshwater rainbow trout and the cost of adaptation to waterborne Zn^{2+}. *J. Exp. Biol.* **198**, 337-348.
Hogstrand, C., Verbost, P. M., Bonga, S. E. W. and Wood, C. M. (1996). Mechanisms of zinc uptake in gills of freshwater rainbow trout: Interplay with calcium transport. *Am J Physiol. Reg I* **39**, R1141-R1147.
Hossain, A. and Dutta, H. (1996). Phylogeny, ontogeny, structure and function of digestive tract appendages (caeca) in teleost fish. In *Fish Morphology* (ed. H. M. Dutta), pp. 59-76. Taylor Francis.
Hwang, P.-P., Lee, T.-H. and Lin, L.-Y. (2011). Ion regulation in fish gills: recent progress in the cellular and molecular mechanisms. *AJP Regul. Integr. Comp. Physiol* **301**, R28-R47.
Jansson, B. and Olsson, R. (1960). The cytology of the caecal epithelial cells of Perca. *Acta Zool.* **41**, 267-276.
Kapoor, B., Smit, H. and Verighina, I. (1976). The alimentary canal and digestion in teleosts. In *Advances in Marine Biology*, Vol. 13 (ed. F. S. Russel and M. Yonge), pp. 109-239. Academic Press.
Karnaky, K. J. (1986). Structure and function of the chloride cell of *Fundulus heteroclitus* and other teleosts. *Integr. Comp. Biol.* **26**, 209-224.
Klaren, P. H. M., Flik, G., Lock, R. A. C. and Wendelaar Bonga, S. E. (1993). Ca^{+2} transport across intestinal brush border membranes of the cichlid teleost *Oreochromis mossambicus*. *J. Membr. Biol.* **132**, 157-166.
Klinck, J. S., Singh, A. and Wood, C. M. (2012). *In vitro* characterization of calcium transport along the gastrointestinal tract of freshwater rainbow trout *Oncorhynchus mykiss*. *J. Fish Biol.* **81**, 1-20.
Larsson, D., Lundgren, T. and Sundell, K. (1998). Ca^{2+} uptake through voltage-gated L-type Ca^{2+} channels by polarized enterocytes from Atlantic cod *Gadus morhua*. *J. Membr. Biol.* **164**, 229-237.
Li, Z., Lui, E. Y., Wilson, J. M., Ip, Y. K., Lin, Q., Lam, T. J. and Lam, S. H. (2014). Expression of key ion transporters in the gill and esophageal-gastrointestinal tract of euryhaline Mozambique tilapia *Oreochromis mossambicus* acclimated to fresh water, seawater and hypersaline water. *PLoS One* **9**, e87591.
Marier, J. R., Neri, L. C., Anderson, T. W. (1979). Water hardness, human health, and the importance of magnesium. NRCC Publication No. 7581. National Research Council of Canada.
Marshall, W. and Grosell, M. (2006). Ion transport, osmoregulation, and acid–base balance. In *The Physiology of Fishes*, Vol. 3 (ed. S. Edwards and D. H. Evans), pp. 179-230. CRC Press.
McCormick, S. D. (1995). Hormonal control of gill Na^+,K^+-ATPase and chloride cell function. In *Cellular and Molecular Approaches to Fish Ionic Regulation* (ed. C. Wood and T. Shuttleworth), pp. 285-315. Academic Press.
Mommsen, T. P. (1984). Biochemical characterization of the rainbow trout gill. *J. Comp. Physiol. B* **154**, 191-198.
Mommsen, T. P., French, C. J. and Hochachka, P. W. (1980). Sites and patterns of protein and amino acid utilization during the spawning migration of salmon. *Can. J. Zool.* **58**, 1785-1799.
Mommsen, T. P., Osachoff, H. L. and Elliott, M. E. (2003). Metabolic zonation in teleost gastrointestinal tract: Effect of fasting and cortisol in tilapia. *J. Comp. Physiol. B Biochem. Syst. Environ. Physiol.* **173**, 409-418.
Nguyen, H. and Donini, A. (2010). Larvae of the midge *Chironomus riparius* possess two distinct mechanisms for ionoregulation in response to ion-poor conditions. *Am. J. Physiol. Integr. Comp. Physiol.* **299**, R762-R773.
Ostos Garrido, M. V., Núñez Torres, M. V. and Abaurrea Equisoain, M. A. (1993). Lipid absorption by enterocytes of the rainbow trout, *Oncorhynchus mykiss*: diet-induced changes in the endomembranous system. *Aquaculture* **110**, 161-171.
Perry, S. F. and Flik, G. (1988). Characterization of branchial transepithelial calcium fluxes in freshwater trout, *Salmo gairdneri*. *Am. J. Physiol.* **254**, R491-R498.
Perry, S. F. and Walsh, P. J. (1989). Metabolism of isolated fish gill cells: contribution of epithelial chloride cells. *J. Exp. Biol.* **144**, 507-520.
Polakof, S., Álvarez, R. and Soengas, J. L. (2010). Gut glucose metabolism in rainbow trout: implications in glucose homeostasis and glucosensing capacity. *Am. J. Physiol. Regul. Integr. Comp. Physiol.* **299**, R19-R32.
Ransberry, V. E., Morash, A. J., Blewett, T. A., Wood, C. M. and McClelland, G. B. (2015). Oxidative stress and metabolic responses to copper in freshwater- and seawater-acclimated killifish, *Fundulus heteroclitus*. *Aquat. Toxicol.* **161**, 242-252.
Rheault, M. R. and O'Donnell, M. J. (2001). Analysis of epithelial K^+ transport in Malpighian tubules of *Drosophila melanogaster*: evidence for spatial and temporal heterogeneity. *J. Exp. Biol.* **204**, 2289-2299.
Rubino, J. G., Zimmer, A. M. and Wood, C. M. (2014). An *in vitro* analysis of intestinal ammonia handling in fasted and fed freshwater rainbow trout (*Oncorhynchus mykiss*). *J. Comp. Physiol. B.* **184**, 91-105.
Schoenmakers, T. J. M., Verbost, P. M., Flik, G. and Bonga, S. E. W. (1993). Transcellular intestinal calcium transport in freshwater fish and its dependence on sodium/calcium exchange. *J. Exp. Biol.* **176**, 195-206.
Schwarz, D. E. and Allen, P. J. (2014). Effects of salinity on growth and ion regulation of juvenile alligator gar *Atractosteus spatula*. *Comp. Biochem. Physiol. A Mol. Integr. Physiol.* **169**, 44-50.
Scott, G. R., Schulte, P. M. and Wood, C. M. (2006). Plasticity of osmoregulatory function in the killifish intestine: drinking rates, salt and water transport, and gene expression after freshwater transfer. *J. Exp. Biol.* **209**, 4040-4050.

Shahsavarani, A. (2006). Characterization of a branchial epithelial calcium channel (ECaC) in freshwater rainbow trout (*Oncorhynchus mykiss*). *J. Exp. Biol.* **209**, 1928-1943.
Sire, M. F., Lutton, C. and Vernier, J. M. (1981). New views on intestinal absorption of lipids in teleostean fishes: an ultrastructural and biochemical study in the rainbow trout. *J. Lipid Res.* **22**, 81-94.
Soengas, J. L., Aldegunde, M. and Andres, M. (1995a). Gradual transfer to sea water of rainbow trout: effects on liver carbohydrate metabolism. *J. Fish Biol.* **47**, 466-478.
Soengas, J. L., Barciela, P., Aldegunde, M. and Andres, D. (1995b). Gill carbohydrate metabolism of rainbow trout is modified during gradual adaptation to sea water. *J. Fish Biol.* **46**, 845-856.
Turner, L. A. and Bucking, C. (2017). The interactive effect of digesting a meal and thermal acclimation on maximal enzyme activities in the gill, kidney, and intestine of goldfish (*Carassius auratus*). *J. Comp. Physiol. B Biochem. Syst. Environ. Physiol.* **187**, 959-972.
Usher, M., Talbott, C. and Eddy, F. (1991). Intestinal water transport in juvenile Atlantic salmon (*Salmo salar* L.) during smolting and following transfer to seawater. *Comp. Biochem. Physiol. Part A Physiol.* **100**, 813-818.
Veillette, P. A., White, R. J., Specker, J. L. and Young, G. (2005). Osmoregulatory physiology of pyloric ceca: regulated and adaptive changes in chinook salmon. *J. Exp. Zool. A. Comp. Exp. Biol.* **303**, 608-613.
Verbost, P. M., Flik, G., Lock, R. A. and Wendelaar Bonga, S. E. (1987). Cadmium inhibition of Ca^{2+} uptake in rainbow trout gills. *Am. J. Physiol.* **253**, R216-R221.
Vijayan, M., Morgan, J., Sakamoto, T., Grau, E. and Iwama, G. (1996). Food-deprivation affects seawater acclimation in tilapia: hormonal and metabolic changes. *J. Exp. Biol.* **199**, 2467-2475.
Whittamore, J. M. (2012). Osmoregulation and epithelial water transport: Lessons from the intestine of marine teleost fish. *J. Comp. Physiol. B Biochem. Syst. Environ. Physiol.* **182**, 1-39.
Williams, J. A. and Nickol, B. B. (1989). Histological structure of the intestine and pyloric ceca of the green sunfish, *Lepomis cyanellus* Rafinesque. *J. Fish Biol.* **35**, 359-372.
Wilson, R., Gilmour, K., Henry, R. and Wood, C. (1996). Intestinal base excretion in the seawater-adapted rainbow trout: a role in acid-base balance? *J. Exp. Biol.* **199**, 2331-2343.
Wood, C. M. and Laurent, P. (2003). Na^+ versus Cl^-transport in the intact killifish after rapid salinity transfer. *Biochim. Biophys. Acta Biomembr.* **1618**, 106-119.
Yu, A. S. L., Cheng, M. H. and Coalson, R. D. (2010). Calcium inhibits paracellular sodium conductance through claudin-2 by competitive binding. *J. Biol. Chem.* **285**, 37060-37069.
Zizza, S. and Desantis, S. (2011). Morphology and lectin-binding sites of pyloric caeca epithelium in normal and GnRH-treated Atlantic bluefin tuna (*Thunnus thynnus*) Linnaeus 1758. *Microsc. Res. Tech.* **74**, 863-873.

Table S1. Summary of Series preparations, site of measurement, and saline compositions.

Feeding Status and Water Treatment	Caeca Portion (proximal to distal) and section (anterior to posterior)	Saline Composition	
		Mucosal Saline	Serosal Saline
Asymmetrical Series			
Unfed - Freshwater	Proximal Anterior, Middle, and Posterior	Cortland Saline (Ca^{2+} concentrations from 0 – 1000 µM)	Cortland Saline (Ca^{2+} concentration 0 µM)
Fed- Freshwater	Proximal Anterior, Middle, and Posterior	Cortland Saline (Ca^{2+} concentrations from 0 – 1000 µM)	Cortland Saline (Ca^{2+} concentration 0 µM)
Fed - IPW	Proximal Anterior, Middle, and Posterior	Cortland Saline (Ca^{2+} concentrations from 0 – 1000 µM)	Cortland Saline (Ca^{2+} concentration 0 µM)
Symmetrical Series			
Unfed - Freshwater	Proximal, Mid, and Distal Anterior, Middle, and Posterior	Cortland Saline (Ca^{2+} concentrations from 0 – 1000 µM)	Cortland Saline (Ca^{2+} concentrations from 0 – 1000 µM)
Fed- Freshwater	Proximal Anterior, Middle, and Posterior	Cortland Saline (Ca^{2+} concentrations from 0 – 1000 µM)	Cortland Saline (Ca^{2+} concentrations from 0 – 1000 µM)
Fed - IPW	Proximal Anterior, Middle, and Posterior	Cortland Saline (Ca^{2+} concentrations from 0 – 1000 µM)	Cortland Saline (Ca^{2+} concentrations from 0 – 1000 µM)

See Materials and Methods for Cortland Saline composition.
Positive flux values indicate absorption by the tissue from the mucosal bath, negative flux values indicate secretion to the mucosal bath.
Osmolality was maintained between the tissue and the baths with appropriate concentrations of mannitol.

Figure S1. Schematic of caeca sampling and Ca^{2+} measurements using ion selective microelectrodes (ISMEs). Caeca were sampled from three locations along the anterior-posterior axis of the anterior intestine: the anterior, the middle, and the posterior. Each caecum was removed, everted, and placed into petri dishes for measurements with ISMEs at the mucosal surface. Ca^{2+} fluxes were measured along the proximal-distal axis of the caeca. The solution in the petri dish was controlled and altered according to each experiment, as was the solution inside the caecum (See Table S1).